Soft Matter

Cite this: *Soft Matter*, 2012, **8**, 1547

www.rsc.org/softmatter

PAPER

Origin of suppressed demixing in casein/xanthan mixtures

Kitty van Gruijthuijsen,[a] Vishweshwara Herle,†[b] Remco Tuinier,[c] Peter Schurtenberger[d] and Anna Stradner*[d]

Received 16th September 2011, Accepted 14th November 2011
DOI: 10.1039/c1sm06761c

We explore the properties of casein/xanthan mixtures for xanthan concentrations beyond those inducing phase separation. Previous work has successfully described the onset of demixing by depletion theory in the protein limit, where the xanthan polysaccharides, the polymers, are larger than the caseins from skim milk powder, the colloids (S. Bhat *et al.*, *J. Phys.: Condens. Matter*, 2006, L339). We now extend these studies to xanthan concentrations in a range of $c/c^* = 13$–88, aiming to arrest the phase separation *via* a (transiently) arrested casein-rich phase. Surprisingly, we find that the casein-rich phase remains fluidic deep into the two-phase region, with an equilibrium composition that significantly differs from predictions for mixtures of hard spheres plus flexible polymer chains in a good solvent. Furthermore, we show that macroscopic phase separation is arrested for $c/c^* > 60$. Our investigations reveal that the rheological properties of the mixtures are fully determined by the xanthan-rich phase with characteristic long relaxation times that depend remarkably strongly on the xanthan concentration.

Introduction

Many food products consist of mixtures of polysaccharides and proteins, which determine their structure, texture, and sensory properties. Above certain polysaccharide concentrations these mixtures tend to phase separate into polysaccharide-rich and protein-rich phases,[1–7] which reduces the visual attractiveness and pleasant mouth feel of the product. In order to design and process food materials it is thus essential to gain a thorough understanding of the parameters governing such demixing processes and to develop strategies to avoid them.

Unfortunately, the tendency of colloid/polymer mixtures to phase separate is inherent to these systems because of the depletion effect; the steric exclusion of the polymer from an area around the colloid results in an effective attraction between the colloids, which in turn leads to phase separation.[8,9] Typically, a dense colloid phase with considerably slower dynamics than the polymer phase is formed.[10] For colloid/polymer mixtures, where the radius of gyration of the polymer R_g is significantly smaller than the radius of the colloid $R_{colloid}$, such phase separation can become arrested when the colloid-rich phase reaches the critical density of an attractive glass in a spinodal decomposition process.[11–13] This arrest often leads to a colloidal gel, where the mixture remains macroscopically homogeneous, while the system is heterogeneous on a microscopic level. Here the dynamically arrested colloid-rich phase forms a space-filling network that resists gravitational stresses.[11–17] This condition prevents the ultimate demixing of the system, which is exploited in food mixtures containing for instance emulsion droplets and polysaccharides, where the size ratio between the polymer and the colloid (droplet) $R_g/R_{colloid}$ is small.[17–20]

In contrast, this ratio is significantly larger in protein/polysaccharide mixtures, such that the depletion attraction becomes longer ranged.[2,3] For long-ranged attractions, however, there is less consensus whether the colloid-rich phase undergoes a true kinetic arrest or to what extent gelation is a transient process.[21] To induce phase separation with larger polymers, they need to be added in such quantities that they approach or surpass their overlap concentration c^*. Therefore, a theoretical description of the equilibrium phase behaviour of such mixtures in the two-phase region needs to take the properties of semi-dilute polymer solutions into account.[22,23] Furthermore, non-equilibrium effects may reveal themselves in concentrated polymer solutions where entanglements become prominent.

We describe our work on mixtures of two commonly used food components, being caseins in the form of micelles as they are present in milk ($R_{colloid} \approx 100$ nm) and renatured xanthan ($R_g \approx 230$ nm). Such mixtures can be considered as colloid/polymer mixtures in the protein regime where $R_g/R_{colloid} > 1$.[1] Caseins form the major fraction of milk proteins. The static and dynamic properties of casein dispersions are well described by concepts used for polydisperse hard sphere colloids up to high concentrations close to the glass transition.[24–28] Xanthan is a rather stiff polysaccharide that forms helices in aqueous salt solutions. For

[a]*Adolphe Merkle Institute, University of Fribourg, Marly, Switzerland. E-mail: Kitty.vanGruijthuijsen@gmail.com*
[b]*Department of Physics, University of Fribourg, Fribourg, Switzerland*
[c]*Van 't Hoff Laboratory for Physical and Colloid Chemistry, University of Utrecht, Utrecht, The Netherlands*
[d]*Division of Physical Chemistry, University of Lund, SE-221 00 Lund, Sweden. E-mail: Anna.Stradner@fkem1.lu.se*
† Current address: BASF, Ludwigshafen, Germany.

renatured xanthan, *i.e.* a solution of xanthan that is heated above 80 °C and cooled down again, this results in a persistence length of $l_p \approx 120$ nm.[29–31] Above its overlap concentration, xanthan can be modelled as a semi-dilute solution of semi-flexible chains.[1,31,32] As established previously, mixtures of casein and xanthan exhibit phase separation when a well defined concentration of xanthan c is exceeded.[1] The position of the phase separation boundary is consistent with that expected for a depletion system. The expected values for the phase coexistence curve obtained from osmotic equilibrium theory for mixtures of hard-sphere colloids and flexible polymer chains in a good solvent are denoted as the drawn line in Fig. 1. We now extend the investigations performed before to explore the behaviour of systems that are deeply quenched into the phase separation region within a range of xanthan concentrations $c/c^* = 13$–88. It is tempting to assume that our casein/xanthan mixtures will show the typical features of depletion systems, where the strongly slowed-down dynamics of the colloid-rich phase permanently or transiently arrest the microscopically phase separated system.

In this paper we show that visual phase separation in casein/xanthan mixtures is indeed suppressed once the xanthan concentration reaches $c/c^* > 60$. Surprisingly, though, we find experimental evidence that this arrest of the demixing process is purely caused by the specific properties of the xanthan-rich phase. We support these findings by a characterization of the rheological properties of xanthan. Finally, we will discuss the implications for the casein-rich phase.

Materials and methods

Materials

The anionic food grade polysaccharide, xanthan (Keltrol T), was a gift from CP Kelko Co. Ltd ($M_w = 4 \times 10^6$ g mol^{-1}, $R_g =$ 230 nm, $c^* = 0.08$ g L^{-1}).[1,31] Low heat grade skim milk powder (SMP) was provided by Hochdorf Swiss Milk AG. It contained 33 wt% total protein, the majority of which was casein (28 wt%). Polystyrene sulfonate particles (Polysciences, diameter 457 nm, concentration 2.5%), sodium azide (Fluka) and sodium chloride (Reactolab) were used without further purification.

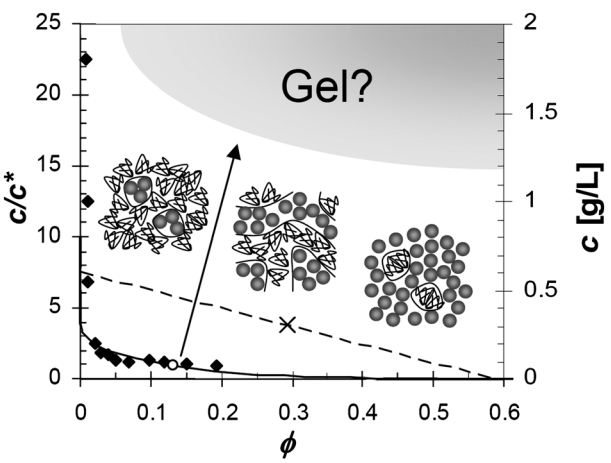

Fig. 1 Phase diagram of casein/xanthan mixtures adopted from ref. 1, where the concentration of xanthan c is given in units of its overlap concentration c^*, and ϕ indicates the casein volume fraction. At the lowest concentrations the samples form homogeneous mixtures, and above the experimental coexistence curve (◆) the mixtures phase separate. The theoretical coexistence curve is shown as a full line with (○) the critical point, and (dashed line) a representative tie line with (×) the midpoint.[1] The schematics show typical micro-structures when phase separation proceeds *via* spinodal decomposition.

Sample preparation

Stock solutions of 15 g L^{-1} xanthan were prepared in 0.1 M NaCl *via* swelling overnight at room temperature, followed by 3 h magnetic stirring at 85 °C. The salt was added to screen the charges on xanthan.

Stock solutions of 30 wt% SMP were prepared by slow addition of SMP to stirred Milli-Q water at 55 °C. This is significantly higher than the concentration of SMP in reconstituted milk (10 wt%[33]). From a stock solution of 30 wt% SMP skim milk permeate was filtered out using a Vivaflow 50 ultrafiltration unit (Sartorious AG) with a 10 kDa molecular weight cut off. The skim milk permeate consisted of salts, lactose, and whey proteins (all <5 nm), and can be considered as the solvent for the casein. The initial volume fraction of casein, ϕ_{ini}, was calculated using eqn (1):

$$\phi_{ini} = c_c \rho \upsilon \quad (1)$$

Here c_c is the casein concentration in g per g, υ is the voluminosity of casein (4.4 mL g^{-1}, ref. 34), and ρ (g mL^{-1}) is the density of the SMP solution as measured with a density and sound analyser (DSA500, Anton Paar). For ρ we determined empirical relations for a background medium consisting of skim milk permeate only, eqn (2), and for a 1 : 1 mixture of skim milk permeate and 0.1 M NaCl, eqn (3):

$$\rho = 0.50 c_c + 1.0741 \quad (2)$$

$$\rho = 0.42 c_c + 1.0360 \quad (3)$$

To all mixtures 2 mM sodium azide was added to prevent microbial growth. Mixtures of casein and xanthan were prepared by 1 : 1 mixing (MS1 Minishaker, IKA) of the corresponding stock solutions, which were diluted from the main stock solutions with skim milk permeate and 0.1 M NaCl respectively. Unless stated otherwise, xanthan concentrations c are expressed in g per L of the total mixture and normalized by the overlap concentration, $c^* = 0.08$ g L^{-1}.

Confocal laser-scanning microscopy

A Leica SP5 confocal laser-scanning microscope (CLSM) was operated in the upright mode (D6000) with a 63× water-immersion objective. The protein phase was non-covalently dyed with 0.01 g L^{-1} Rhodamine B (excitation at 561 nm). After mixing the samples by vortexing, a drop was applied to a microscope slide and fixed with a spacer (Secure-Seal imaging spacer, Sigma, 0.12 mm thickness, window diameter 13 mm) under a cover glass (Corning, #1½ , 22 × 22 mm^2). A square pixel slice was taken (512 × 512) with image dimensions of 146 × 146 μm. Images were scanned approximately 10–20 μm below the

level of the cover glass to minimize hydrodynamic interactions with the cover glass.

Rheometry

Dynamic rheology measurements were performed with a strain controlled ARES-LS1 rheometer (TA instruments). After being mixed, the samples were centrifuged at 1000 rpm for 5 min to remove air bubbles. Measurements were carried out with a plate–cone geometry (50 mm diameter, 0.04 rad angle, 0.0438 mm gap) in combination with a solvent trap and thermostatted at 25 °C. In all oscillation measurements a 1% strain was applied, which was within the linear regime for all samples. To let the mixtures equilibrate, they were first measured at 10 rad s^{-1} for 1–2 h, after which a frequency sweep (100–0.01 rad s^{-1}) was recorded.

Diffusing wave spectroscopy

Echo two-cell Diffusing Wave Spectroscopy (DWS) experiments in transmission geometry were performed as described previously.[35] Typical measurement times were in the range of 3–5 min. Samples were measured at 25 °C in standard glass cuvettes (Hellma) with a path length L of 10 mm and a width of 15 mm. 1–2% polystyrene particles (diameter 457 nm) in water ($T = 25$ °C, $\eta = 0.89$ mPa) were used as a reference to determine l^* (photon transport mean free path) from the transmitted intensities $I_{transmitted}$ according to eqn (4):

$$\frac{I_{transmitted}}{I_0} = \frac{5L/3l^*}{1 + 4L/3l^*} \quad (4)$$

From the DWS intensity correlation function $g_2(t)$ the ensemble averaged particle mean square displacement $\langle \Delta r^2(t) \rangle$ was obtained assuming the diameter of the illuminating extended beam $d > L$ ($d = 12$ mm), and $L/l^* \gg 1$ (eqn (5)–(7)):[36]

$$g_1(t) = \sqrt{\frac{g_2(t) - 1}{\beta}} \quad (5)$$

$$g_1(t) = \frac{((L/l^*) + (4/3))\sqrt{Q}}{(1 + (8t/3\tau))\sin h[(L/l^*)\sqrt{Q}] + 4/3\sqrt{Q}\cos h[(L/l^*)\sqrt{Q}]} \quad (6)$$

with

$$Q = k_0^2 \langle \Delta r^2(t) \rangle \quad (7)$$

Here $g_1(t)$ is the electric field correlation function, β an experimental set-up parameter, and the wave vector $k_0 = 2\pi n/\lambda$, with $n = 1.33$ the refractive index of the solvent and $\lambda = 633$ nm the wavelength of the laser. It was verified that the results are in agreement with those for a limited beam width ($d \approx L$).[36] All data analyses were performed using the software package DWS-Rheolab (LS Instruments).

Results and discussion

Phase diagram

To investigate the possibility of gelation in casein/xanthan mixtures, we studied the phase-separation behaviour of xanthan concentrations beyond the previously determined coexistence line.[1] Fig. 2 shows the composition of the studied mixtures in the extended phase diagram of Fig. 1. We started each experiment by vortexing the samples for 1 min. This procedure ensured that the samples were homogenized even though mixing at a molecular level was most likely not achieved. We followed the evolution of the samples for several months by visual observation and confocal microscopy.

Our visual observations directly subdivided the samples in those with $c/c^* < 60$ that ultimately fully phase separated, denoted as open triangles in Fig. 2, and those with $c/c^* > 60$ that remained macroscopically mixed over several months, depicted as closed triangles. For $c/c^* < 60$ a white casein-rich sediment appeared within several hours, which grew *via* further sedimentation of visible white domains with a finite size. For $c/c^* = 13$ the sediment stopped growing after approximately 24 h, at which time the upper xanthan-rich phase was almost transparent.

Although for $c/c^* = 38$ the majority of the casein-rich phase sedimented within 24 h as well, full sedimentation took several weeks.

Using the fully sedimented samples, we estimated the casein volume fraction in the casein-rich phase, ϕ_{CRP}, assuming that the amount of casein in the xanthan-rich phase was negligible. This is justified since the upper phases of these systems were almost transparent. In this case, ϕ_{CRP} can be deduced from the ratio between the height of the casein-rich phase and that of the total sample, $r_h = h_{CRP}/h_{total}$, and the initial casein content ϕ_{ini}, according to $\phi_{CRP} = \phi_{ini}/r_h$. We verified that the r_h values did not show further changes with time. Furthermore, we assumed that the two phases reached their equilibrium compositions and that these compositions are an extension of the phase diagram for lower xanthan concentrations. This implies that c/c^* in the casein-rich phase does not exceed values around unity, which can be neglected compared to the xanthan concentration in the xanthan-rich phase. The results are shown in Fig. 2 as tie lines. To test the latter assumption, we estimated the xanthan

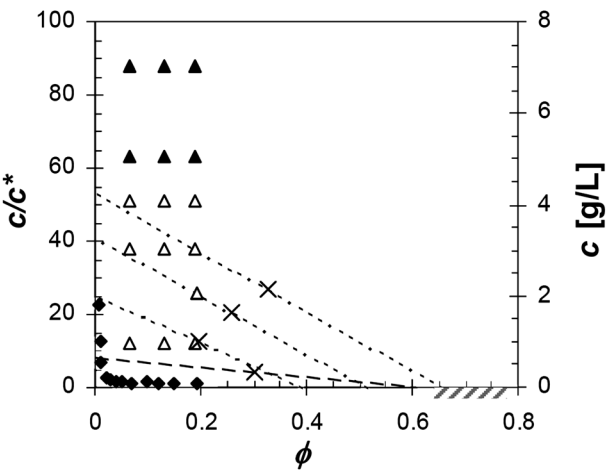

Fig. 2 Phase diagram of casein/xanthan mixtures depicting the studied samples that fully phase separate (△) or appear homogeneous over months (▲). The experimental coexistence curve (◆) is redrawn from ref. 1 for comparison. The dotted and dashed lines correspond to respectively experimental and theoretical tie lines with their midpoints (×). The dashed area denotes the glass transition for pure casein.[25,26]

concentration in the casein-rich phase based on the measured ϕ_{CRP} values and the theoretical free volume assuming the mesh size of the xanthan network to scale with $\sim(c/c^*)^{-3/4}$. We find c/c^* values in the casein-rich phase of 4–8, which would slightly flatten the experimental tie lines. As we will discuss later on, the xanthan mesh size rather scales with $\sim(c/c^*)^{-1/2}$, in which case the estimated xanthan concentration in the casein-rich phase would be truly negligible.

Surprisingly, the thus determined experimental tie lines have much steeper slopes than the theoretically predicted tie line in Fig. 1; to reach $\phi_{CRP} \approx 0.6$ the concentration of xanthan must be almost a factor of 7 larger than theoretically predicted. Note that we used an upper estimate of the casein voluminosity to calculate ϕ_{ini}. At high osmotic pressures caseins can show some deswelling, which would result in even lower values for ϕ_{ini} and ϕ_{CRP}.[34,37] Thus, our findings show that the extrapolation of typical features of colloid/polymer mixtures truly overestimates the densification of the casein-rich phase. This is in so far surprising as several studies have shown that the theory correctly captures the experimental coexistence curves for colloid/polymer mixtures in the protein regime,[2] including the coexistence curve of casein/xanthan mixtures.[1] Typically, such experimental curves are determined at the onset of demixing, rather than by the composition of two coexisting phases, *i.e.* the tie lines. Our findings thus may indicate that the theory for depletion induced phase separation in the protein limit has to be reconsidered. However, as will be discussed later, casein/xanthan mixtures cannot be regarded as simple colloid/polymer mixtures for c above c^*, such that the observed discrepancy may also be specific to our system rather than generic for colloid/polymer mixtures in the protein limit.

Besides denoting the composition of coexisting phases, tie lines also indicate the volume ratio between the two phases. The microscopic evolution of phase separation is linked to this ratio, as shown by the schematics in Fig. 1. Exactly half-way the tie lines the volumes of the two phases are equal. After quenching at such a location in the phase diagram one expects the formation of a bicontinuous network in the early stages of spinodal decomposition. For compositions closer to the binodal the formation of a space-spanning network by the minority phase is less likely. Here the minority phase is expected to appear as droplets in a continuous background of the majority phase. We tested this scenario for the sample with $\phi_{ini} = 0.19$ and $c/c^* = 25$. Indeed, the confocal images initially showed stretched, potentially space-spanning casein-rich domains, coloured in white in Fig. 3. Subsequently, the domains fused into larger, spherical droplets that ultimately sedimented onto the microscope slide. This microscopic onset of phase separation agrees with expectations when treating our system as a typical colloid/polymer mixture.[12,17,38]

The temporal evolution of the microscopic phase separation of all systems under study showed comparable features during the first 20 min: the casein-rich phase started as stretched domains, evolving into more spherical droplets, albeit with a slower evolution with increasing xanthan concentration. Interestingly, all systems with $c/c^* < 60$ kept evolving, as shown for $c/c^* = 25$ in Fig. 3. In contrast, for all systems with $c/c^* > 60$ the relaxation of casein-rich domains effectively stopped after 20 min. Moreover, the domains showed no further minimization of the interface and seemed to be fixed in space.

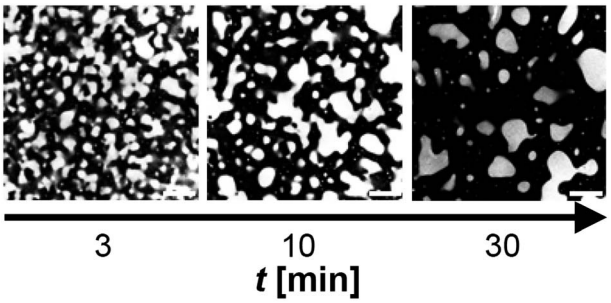

Fig. 3 Time evolution after initialisation of a casein/xanthan mixture with $\phi = 0.19$ and $c/c^* = 25$ shown as CLSM images in the horizontal plane. Casein is dyed with rhodamine and shown in white. Scale bars are 25 μm.

To verify whether these clear differences in the evolution of the micro-domains led to distinguishable static structures, 2D images of all samples were compared 2 h after mixing, as shown in Fig. 4. The schematic shows the position of the images in the sample volume. Indeed, the mixtures with $c/c^* = 13$ and $\phi_{ini} = 0.13$ and 0.19 had sufficiently sedimented yielding fully black images. Focussing lower in the sample volume, the sedimented casein-rich phase appeared homogeneously white, which implies that no xanthan-rich domains were left in the sediment. Surprisingly, the other samples in Fig. 4 almost all showed spherical casein-rich domains dispersed in a continuous xanthan-rich background,

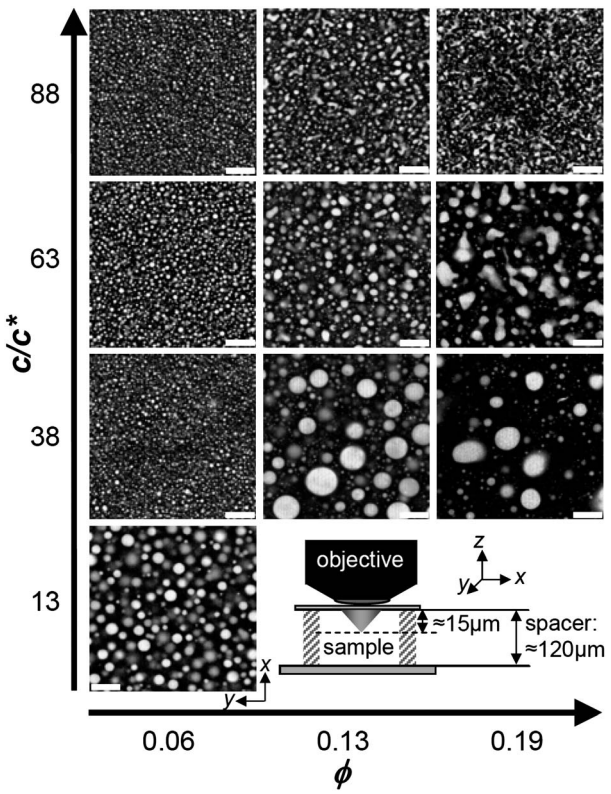

Fig. 4 Phase diagram of casein/xanthan mixtures 2 h after initialisation shown as CLSM images in the horizontal plane, as depicted in the schematic. The two missing images appeared fully black. Casein is dyed with rhodamine and shown in white. Scale bars are 25 μm.

where the droplet size decreased with increasing xanthan concentration or decreasing casein content. Only for the samples with $c/c^* = 63$ and 88 and $\phi_{ini} = 0.19$, and with $c/c^* = 88$ and $\phi_{ini} = 0.13$ the casein-rich domains were somewhat stretched. Compiled 3D-stacks of these samples showed disconnected casein-rich phases, except for $c/c^* = 88$ and $\phi_{ini} = 0.19$ (results not shown). Therefore, the macroscopically observed arrest did not show any correlation with the structure of the casein-rich domains, but rather with the motional freedom of these domains in the xanthan background. This implies that in our casein/xanthan mixtures it is the polymer-rich phase that exhibits the slowest dynamics and causes the macroscopic arrest. It thus opposes the route to gelation discussed in the Introduction, where the slow dynamics of the colloid-rich phase tend to arrest phase separating mixtures in which the polymer is significantly smaller than the colloid.

In summary, we have observed unexpectedly low equilibrium casein concentrations in our visually phase separating samples compared to existing theoretical predictions. Most importantly, we have found strong indications that the xanthan-rich phase causes an arrest of the phase separation process for $c/c^* > 60$.

Mechanical properties

To elucidate the latter observation, we characterized the mechanical properties of mixtures with $\phi_{ini} = 0.13$ and $c/c^* = 38$–88 1–2 h after the initialization step. The frequency dependence of the loss modulus, G'', and storage modulus, G', exhibited typical visco-elastic features; for the lowest xanthan concentration, $c/c^* = 38$, G' dominated at high frequencies, while G' and G'' approached their cross-over point at low frequencies, as shown in Fig. 5(a). With increasing xanthan concentration the cross-over frequency ω_c, where $G' = G''$, shifted to lower frequencies and became too small to be accessible in our experiment with a limited frequency range of $\omega = 0.1$–100 rad s^{-1}.

To accurately determine both the cross-over frequency and the magnitude of the modulus at the cross-over frequency $G_c = G'(\omega_c) = G''(\omega_c)$, we used a scaling procedure; we normalized the frequency with ω_c and both storage and loss moduli with G_c so as to obtain the best overlap of the low-frequency range of each individual dataset on a master-curve, as shown in Fig. 6(a). This master-curve was strikingly similar to that obtained for xanthan solutions in the absence of casein, shown in Fig. 6(b). This similarity strongly suggests that the rheology of the mixtures is predominantly determined by the xanthan-rich phase. Indeed, a comparison between the values obtained for ω_c in terms of structural relaxation times $\tau_R = 2\pi/\omega_c$ as a function of the xanthan concentration, depicted in Fig. 7, led to an almost perfect collapse of both datasets, provided that the xanthan concentration of the mixtures was renormalized to the one within the accessible space, *i.e.* the space not occupied by casein, given by $c/(c^* \cdot (1 - \phi_{ini}))$.

The structural relaxation time τ_R revealed a remarkably strong dependence on the xanthan concentration, which significantly exceeded the scaling typically found in polymers, where relaxation is dominated by reptation with a maximal scaling of $\tau_R \approx (c/c^*)^{7/3}$ for flexible polymers in a θ-solvent.[39] Instead, we

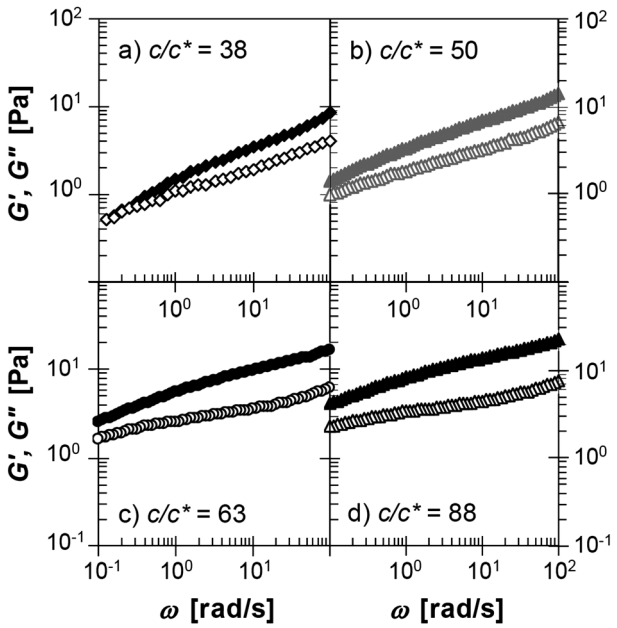

Fig. 5 Storage (G', full symbols) and loss (G'', open symbols) moduli with increasing xanthan concentration in casein/xanthan mixtures with $\phi_{ini} = 0.13$.

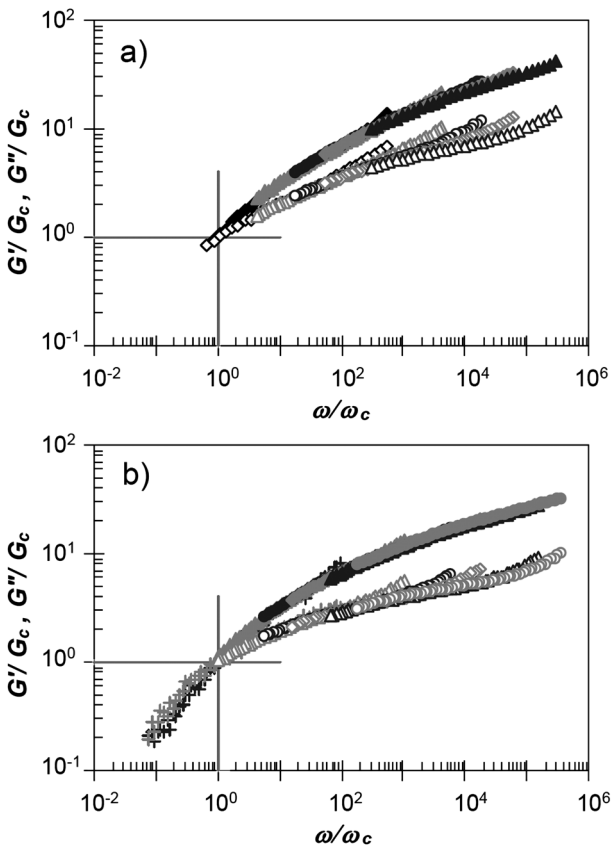

Fig. 6 Superimposed storage and loss moduli of (a) casein/xanthan mixtures with $\phi_{ini} = 0.13$, and (b) xanthan in 1 : 1 0.1 M NaCl/skim milk permeate. Xanthan concentrations in the total mixtures are labelled according to Fig. 5 with G' and G'' respectively black and grey plus signs for $c/c^* = 31$, ▲ and △ for $c/c^* = 100$, and ● and ○ for $c/c^* = 113$.

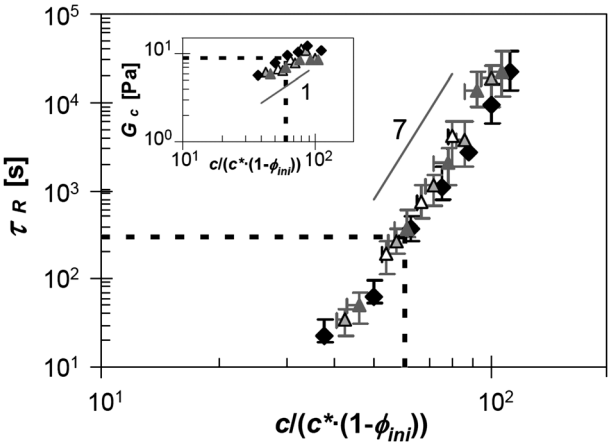

Fig. 7 Extrapolated relaxation time and (inset) cross-over modulus as a function of xanthan concentration in the continuous phase. Symbols denote (filled diamonds) xanthan in 1 : 1 0.1 M NaCl/skim milk permeate, casein/xanthan mixtures with (open triangles) $\phi_{ini} = 0.06$, (black-grey triangles) $\phi_{ini} = 0.13$, and (grey triangles) $\phi_{ini} = 0.19$. Vertical error bars are manually estimated during superposition and horizontal error bars denote a reduction of 35% in the casein voluminosity.[34,37]

found $\tau_R \approx (c/c^*)^7$ which suggests that the relaxation time of xanthan in this concentration range is not simply set by reptation. Such an anomaly has been observed before,[40–43] and is related to the tendency of xanthan to form double helices that connect two chains with each other.[42,44,45] These physical cross-links break and reform continuously. If we consider that an increasing portion of xanthan will be trapped in double helices as the concentration increases, such non-linear increase in the number of double helices would account for the remarkable increase of τ_R with xanthan concentration.

The consequences of this strong increase of τ_R for the use of xanthan as a (food) thickener become tangible when we relate it to the demixing behaviour of our casein/xanthan mixtures. Varying the xanthan concentration in a narrow range of concentrations significantly shifts the structural relaxation time of xanthan. At some critical relaxation time the casein-rich domains become permanently trapped in the xanthan continuous phase, such that the system remains macroscopically homogeneous over an extended period of time. Indeed, we observe suppressed demixing for relaxation times longer than 3×10^2 s, which is close to the typical relaxation time related to glass transitions of 10^2 s. Thus far, we have allocated the arrest transition at $c/c^* = 60$. Yet, the adjusted x-axis in Fig. 7 suggests that if we would draw an arrest line in Fig. 2, it would be tilted such that the xanthan concentration in the free volume would be constant. However, we have not sufficiently zoomed in on this part of the phase diagram to determine the exact location of the arrest line.

Osmotic pressure and mesh size of xanthan

In the osmotic equilibrium theory used in Fig. 1 the key ingredients are the polymer concentration-dependent osmotic pressure and depletion thickness, derived for flexible chains in a good solvent in the presence of monodisperse pure hard spheres. It is questionable to which extent these theoretical results apply to xanthan. To test these assumptions, we derive estimates of the two key parameters from our rheological results.

In the first approach, the plateau elastic modulus G^0 can be related to the osmotic pressure of the polymer solutions, which in turn sets the strength of the depletion attraction between the colloids.[8,9,23] For systems where the elastic modulus does not show a clear plateau, like ours, G^0 can be approximated by the point where G'/G'' is maximal.[46,47] This point denotes the transition from relaxation of single chains in the background solvent at high frequencies to the long-time relaxation characterized by τ_R. As such, the low-frequency cross-over modulus that we determined before, G_c in the inset of Fig. 7, is related to, but not directly proportional to, G^0.

To estimate G^0, we extended the frequency range by diffusing wave-spectroscopy (DWS) micro-rheology. DWS enables us to measure the dynamics of added tracer particles and it relates their mean square displacement $\langle \Delta r^2(t) \rangle$ to the visco-elastic properties of the medium following the generalized Stokes–Einstein equation.[36,48] Here we used tracer particles with $R_{tracer} = 229$ nm. The visco-elastic moduli determined with DWS micro-rheology perfectly overlapped with the rheometry data, as is shown in Fig. 8 for a representative xanthan solution of $c/c^* = 38$. Around the high-frequency cross-over point the frequency dependence of G' and G'' showed a scaling of $\sim\omega^{1/4}$ and $\sim\omega^{3/4}$ respectively, as depicted in Fig. 8. Interestingly, the same scaling factors were previously reported for highly entangled solutions of F-actin, which also behaves as a semi-flexible polymer.[47]

In DWS micro-rheology both G' and G'' are determined from the curvature of the $\langle \Delta r^2(t) \rangle$ curves, where the maximum of G'/G'' corresponds to the inflection point of $\langle \Delta r^2(t) \rangle$. The almost constant slope of $\langle \Delta r^2(t) \rangle$ for the xanthan concentrations under study hampered an accurate determination of the inflection point. The limitation to determine both G' as well as G'' with sufficient accuracy from DWS data also excluded the use of the high-frequency cross-over as a characteristic point. This point fell outside the measurable range for $c/c^* > 50$, and to use a scaling procedure such as the one applied to the low-frequency

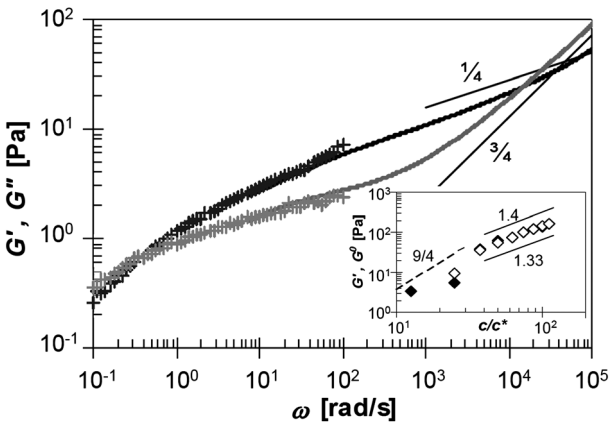

Fig. 8 Visco-elastic moduli G' (black) and G'' (grey) of a xanthan solution with $c/c^* = 38$ measured with rheometry (symbols) and DWS micro-rheology (drawn lines, scaled down by a factor of 1.8). Inset: (◆) G' and (◇) estimated G^0 values at $\omega = 10^4$ rad s^{-1} measured with DWS micro-rheology as a function of xanthan concentration. Thin lines indicate typical scalings for semi-flexible polymer solutions.

cross-over, we would need precise knowledge of both G' and G'' over an extended frequency range.

As a compromise, we determined tangents to the dominant, and thus more accurately determined, elastic modulus with the frequency scaling typical for highly entangled semi-flexible polymers, $G' \approx \omega^{1}/_{4}$. The values of the tangents at $\omega = 10^4$ rad s^{-1} were taken as an indication for G^0. As a comparison, the directly measured values for G' at $\omega = 10^4$ rad s^{-1} are plotted together with the estimated G^0 values in the inset of Fig. 8. The values showed a scaling of $\sim(c/c^*)^{1.38\pm0.06}$, which is in perfect agreement with scaling behaviour for highly entangled semi-flexible polymers.[46,47,49] For the F-actin mentioned before, an experimental scaling of 1.4 was found, compared to a theoretical scaling of 1.33.[47] In contrast, in the less entangled semi-dilute concentration regime, a scaling of $\sim(c/c^*)^{9/4}$ is predicted. Indeed, for $c/c^* < 40$ we observed a steeper scaling, with a larger discrepancy between the two methods, suggesting that the assumption of highly entangled scaling to estimate G^0 is not valid in this concentration range. All in all, this implies that the osmotic pressure of the xanthan solution above the coexistence curve increases with $\sim(c/c^*)^x$, where $x \approx 2$ for $c/c^* < 40$ and $x \approx 1.38$ for $c/c^* > 40$. In the depletion picture, the xanthan osmotic pressure sets the strength of the attraction between the caseins. Our scaling exponents imply that the osmotic pressure increases more than linearly with the xanthan concentration. This in turn suggests the presence of very strong attractions between the caseins in our mixtures. These findings stand in stark contrast to our experimental tie lines in Fig. 2. The unexpected low concentrations of casein in the casein-rich phase suggest much weaker attractions.

To further elucidate the influence of xanthan, we estimated the mesh size ξ of the xanthan solutions. It has been shown that above c^* the mesh size, rather than the polymer radius, determines the second parameter used in the theory, the depletion thickness.[22,23] The mesh size is defined as the typical size of polymer blobs between entanglements, and decreases with increasing polymer concentration. Opposite to the scaling for flexible chains in a good solvent, where $\xi \approx (c/c^*)^{-3/4}$,[39] for semi-flexible polymers ξ only scales with $\sim(c/c^*)^{-1/2}$.[50,51] This implies that the depletion thickness decreases much less than predicted by our theoretical description. Hinsch *et al.* defined the mesh size of highly entangled solutions of semi-flexible polymers by $\xi = \sqrt{3/\upsilon L_c}$, where ν is the number density of polymers with contour length L_c,[51] which is typically found to be $L_c = 2$ μm for renatured xanthan.[29–31] From this we estimated the mesh size to decrease from $\xi \approx 100$ nm to $\xi \approx 30$ nm with increasing xanthan concentrations of $c/c^* = 13$ to $c/c^* = 88$. Compared to the size of caseins, $R_{colloid} = 100$ nm, these estimates suggest that the attractions are not decidedly short-ranged. In such systems gels have been observed before, but are not yet extensively characterized.[2,21]

Next to proving that the dynamics of the xanthan-rich phase induce the arrested phase separation for $c/c^* > 60$, our rheological investigations yielded estimates of the osmotic pressure and the mesh size of the xanthan-rich phase. These properties supposedly determine equilibrium properties of the two phases. Surprisingly, we found a concentration scaling of the osmotic pressure that would predict a much stronger densification of the casein-rich phase than we observed. The estimated range of the attractions, larger than $0.1 \cdot R_{colloid}$, suggested that well-established findings from short-range attractive systems are not applicable to our casein/xanthan mixtures. However, it does not exclude transient gelation, which has previously been observed in longer-range attractive systems as well.[21]

Dynamics of the casein-rich phase

To study the effect of attractions on the casein-rich phase, we measured the dynamics of the caseins, in the form of the mean square displacement $\langle \Delta r^2(t) \rangle$, by DWS. We exploited the fact that the scattering contribution of xanthan is negligible compared to that of casein, to perform the experiments in the mixed state. We investigated two series of samples: in series 1 we maintained the xanthan concentration at $c/c^* = 38$ and varied the casein content in the range of $\phi_{ini} = 0.06$–0.19; in series 2 we maintained the casein concentration at $\phi_{ini} = 0.13$ and varied the xanthan concentration in the range of $c/c^* = 38$–88. As shown in Fig. 4, the systems of both series were not demixed after 2 h waiting time, with the casein being trapped in some droplet phase of varying size.

For series 1 we compared the dynamics measured in the mixed state to those measured in the casein phase after demixing. Our experiments revealed that the dynamics of all samples were essentially indistinguishable, as shown in Fig. 9(a). The almost perfect collapse of data obtained in the mixed phase and the condensed sedimented phase showed that we indeed probed the individual caseins in the casein-rich phase, and that the caseins in this series all experienced comparable environments. The correlation functions fully decayed, which limited the mean square displacement data to shorter times, in which they initially increased linearly with time. These results corroborate our findings from microscopy that the casein-rich domains internally relax on sub-second time scales and are decidedly fluid-like.

In addition, the agreement between samples measured at different stages of the sedimentation process suggests that we look at the equilibrium composition of the casein-rich phase in such mixtures. Indeed, xanthan solutions at $c/c^* = 38$ relaxed on experimentally relevant time scales, as can be read from Fig. 6. All in all, we find an equilibrium casein-rich phase, with a casein concentration that is low compared to what we would expect from the osmotic pressure of the xanthan network. We tentatively argue that the large persistence length of xanthan, together with the onset of double helix formation in the concentration range under study, affects the configuration and the osmotic pressure of our highly entangled xanthan in the confinement between the caseins. Unfortunately, we have not managed to explicitly determine the xanthan concentration in both phases. Nevertheless, the significantly faster dynamics of the caseins compared to tracer particles at comparable overall xanthan concentrations, as visible from Fig. 9(a), confirm that the properties of the solvent in the casein-rich phase are not a direct continuation of those of the xanthan-rich phase.

Finally, to put our data into perspective, we compared series 2, where we varied the xanthan concentration, to a concentration series of casein in skim milk permeate up to volume fractions just below the jamming transition, $\phi = 0.52$ to $\phi = 0.68$. The casein concentration series did not show significant caging effects on the accessible time and length scales in the form of a plateau at longer times, as denoted by the lines in Fig. 9(b). This suggests

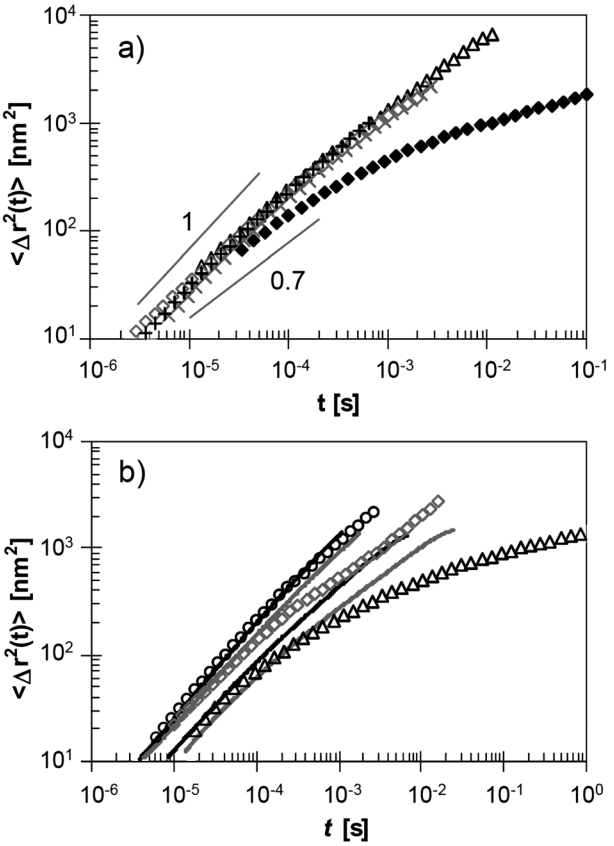

Fig. 9 (a) Mean square displacements determined with DWS for mixtures of casein and xanthan with $c/c^* = 38$. Complete mixtures are measured 2 h after initialisation with $\phi_{ini} = 0.06$ (△), 0.13 (×), and 0.19 (◇). For $\phi_{ini} = 0.13$ the sedimented casein-rich phase is measured after 24 h (+). To enable comparison, the tracer DWS data for a xanthan solution with $c/c^* = 38$ (◆) are rescaled by $R_{tracer}/R_{colloid}$. (b) Mean square displacements determined with DWS 2 h after initialisation, for casein/xanthan mixtures with $\phi_{ini} = 0.13$ and $c/c^* = 38$ (○), 63 (◇), and 88 (△). The lines correspond to casein solutions in skim milk permeate with $\phi =$ 0.52 (black), 0.57 (grey), 0.64 (black), and 0.68 (grey) from left to right.

that the casein solutions were in the fluid state. We were limited by the filtration procedure used to concentrate the caseins, such that we could not reach concentrations at or above the glass transition.[25,26] Next to the specific properties of xanthan that could explain our unexpected phase behaviour, caseins show deviations from hard sphere behaviour as well. There is some evidence that at such high volume fractions the osmotic pressure of casein dispersions is much higher than expected for hard spheres.[25] This would further limit the applicability of our theory.

The long-time dynamics of caseins in some of the mixtures of series 2 showed a significant slowing down compared to the pure caseins, as visible in Fig. 9(b). At short times, the dynamics followed the trends in ϕ_{CRP} with increasing xanthan concentration denoted by the tie lines in Fig. 2. Note that the listed volume fractions strongly depend on the voluminosity which is taken as a constant here, and should therefore be taken as indicative values only.[34,37] Intuitively, we would relate the slowing down at long times to the presence of additional depletion-induced attractions and the onset of an attractive glass transition. A closer look at the data shown in Fig. 9(b) in fact indicates fluid-like dynamics for $c/c^* = 38$, onset of caging for the sample with $c/c^* = 63$, and arrested dynamics with a well developed plateau at $c/c^* = 88$. However, as the plateau in the mean square displacement of colloids critically depends both on the volume fraction and interaction potential, we can currently not comment on the nature of the arrest observed in the sample with the highest xanthan concentration.

Conclusions

We presented experimental data that elucidate two surprising phenomena observed in casein/xanthan mixtures which are deeply quenched into the two-phase region. At xanthan concentrations around c^* such mixtures follow the typical behaviour of colloid/polymer mixtures governed by depletion interactions as described by Generalized Free Volume Theory (GFVT).[1] Upon our deeper quenches, we first demonstrated that demixing of casein/xanthan mixtures is suppressed for xanthan concentrations $c/c^* > 60$. In contrast to colloid/polymer mixtures with short-range attractions, where a particle gel can form that arrests the phase transition, we found that xanthan formed the continuous phase in which casein-rich domains—occupying up to a fifth of the total volume—become effectively trapped. The organisation of xanthan into inter- and intra-molecular helices caused the remarkably strong dependence of the relaxation time on the xanthan concentration.

For shallower quenches of $13 < c/c^* < 60$ we subsequently showed a significant deviation of the theoretically predicted composition of coexisting phases and those found experimentally. Phenomenologically, our systems with $c/c^* < 60$ showed all the typical features of phase separation proceeding *via* spinodal decomposition eventually reaching equilibrium compositions in two fully separated phases. Our estimates of the key quantities to describe the phase behaviour of colloid–polymer mixtures for arbitrary size ratios—being the osmotic pressure of the polymer solution and the depletion thickness for the polymers around the colloids—suggest that xanthan neatly behaved as a semi-flexible polymer. Yet, we find unexpectedly low casein concentrations in the casein-rich phase. We expect that this discrepancy is related to the theoretical assumption that the properties of xanthan in the confined spaces in the casein-rich phase can be described by the properties of xanthan in the bulk continuous phase. Notably the large persistence length of xanthan and its tendency to form double helices will have a strong effect under confinement. Finally, for $c/c^* > 80$ we found signatures of a glassy arrest of the casein-rich phase. However, based on the current data we cannot conclude on the nature of the glass transition that the caseins exhibit.

In summary, mixtures of casein and xanthan, both extensively used as food ingredients, form an interesting system to bridge the knowledge gap from model systems to real (food) products. We have tried to show that current theoretical models start to grasp the added complexity of natural ingredients, but do not yet fully capture the entire phase behaviour. The subsequent application of our understanding of equilibrium phase diagrams to non-equilibrium gel states is therefore implicitly hampered. It would be interesting to compare our results to mixtures of caseins with more ideal polymers, like pullulans, or to mixtures of xanthan

with colloids that behave more like hard spheres.[38] Nevertheless, our rheological findings yield a straightforward tool to estimate properties like shelf life for more complex products based on xanthan. In contrast, our results mostly raise questions about the nature of arrest in colloidal systems with long-range attractions. Further research is needed to shed light on this intriguing issue.

Acknowledgements

K.v.G. thanks Veronique Trappe for numerous intense and useful discussions and for her critical remarks, which considerably improved this manuscript. We are grateful to Suresh Kumar Bhat for many important discussions. Ilja Voets and Corinne Jud are thanked for their comments on the manuscript, and Yuki Umehara for her help in the laboratory. We gratefully acknowledge financial support from the Swiss National Foundation (SNF 200021_119964), the Nestlé Research Center, Lausanne, Switzerland, the University of Fribourg, Switzerland, and the Adolphe Merkle Foundation.

Notes and references

1 S. Bhat, R. Tuinier and P. Schurtenberger, *J. Phys.: Condens. Matter*, 2006, **18**, L339–L346.
2 R. Tuinier, J. K. G. Dhont and C. G. de Kruif, *Langmuir*, 2000, **16**, 1497–1507.
3 P. W. de Bont, G. M. P. van Kempen and R. Vreeker, *Food Hydrocolloids*, 2002, **16**, 127–138.
4 H. M. Schaink and J. A. M. Smit, *Food Hydrocolloids*, 2007, **21**, 1389–1396.
5 M. Corredig, N. Sharafbafi and E. Kristo, *Food Hydrocolloids*, 2011, **25**, 1833–1841.
6 V. Y. Grinberg and V. B. Tolstoguzov, *Food Hydrocolloids*, 1997, **11**, 145–158.
7 J. L. Doublier, C. Garnier, D. Renard and C. Sanchez, *Curr. Opin. Colloid Interface Sci.*, 2000, **5**, 202–214.
8 A. Vrij, *Pure Appl. Chem.*, 1976, **48**, 471–483.
9 H. N. W. Lekkerkerker, W. C. K. Poon, P. N. Pusey, A. Stroobants and P. B. Warren, *Europhys. Lett.*, 1992, **20**, 559–564.
10 T. Moschakis, B. S. Murray and E. Dickinson, *Langmuir*, 2006, **22**, 4710–4719.
11 W. C. K. Poon, A. D. Pirie and P. N. Pusey, *Faraday Discuss.*, 1995, 65–76.
12 N. A. M. Verhaegh, D. Asnaghi, H. N. W. Lekkerkerker, M. Giglio and L. Cipelletti, *Phys. A*, 1997, **242**, 104–118.
13 P. J. Lu, E. Zaccarelli, F. Ciulla, A. B. Schofield, F. Sciortino and D. A. Weitz, *Nature*, 2008, **453**, 499–504.
14 F. Cardinaux, T. Gibaud, A. Stradner and P. Schurtenberger, *Phys. Rev. Lett.*, 2007, **99**, 118301.
15 T. Gibaud and P. Schurtenberger, *J. Phys.: Condens. Matter*, 2009, **21**, 322201.
16 H. Tanaka, Y. Nishikawa and T. Koyama, *J. Phys.: Condens. Matter*, 2005, **17**, L143–L153.
17 T. Moschakis, B. S. Murray and E. Dickinson, *J. Colloid Interface Sci.*, 2005, **284**, 714–728.
18 M. A. Faers and G. R. Kneebone, *Pestic. Sci.*, 1999, **55**, 312–325.
19 Y. Hemar, M. Tamehana, P. A. Munro and H. Singh, *Food Hydrocolloids*, 2001, **15**, 513–519.
20 A. Parker, P. A. Gunning, K. Ng and M. M. Robins, *Food Hydrocolloids*, 1995, **9**, 333–342.
21 L. J. Teece, M. A. Faers and P. Bartlett, *Soft Matter*, 2011, **7**, 1341–1351.
22 G. J. Fleer and R. Tuinier, *Phys. Rev. E: Stat., Nonlinear, Soft Matter Phys.*, 2007, **76**, 041802.
23 G. J. Fleer and R. Tuinier, *Adv. Colloid Interface Sci.*, 2008, **143**, 1–47.
24 M. Alexander, L. F. Rojas-Ochoa, M. Leser and P. Schurtenberger, *J. Colloid Interface Sci.*, 2002, **253**, 35–46.
25 A. Bouchoux, B. Debbou, G. Gesan-Guiziou, M. H. Famelart, J. L. Doublier and B. Cabane, *J. Chem. Phys.*, 2009, **131**, 165106.
26 L. Dahbi, M. Alexander, V. Trappe, J. K. G. Dhont and P. Schurtenberger, *J. Colloid Interface Sci.*, 2010, **342**, 564–570.
27 C. G. de Kruif, *J. Dairy Sci.*, 1998, **81**, 3019–3028.
28 C. G. de Kruif and C. Holt, in *Advanced Dairy Chemistry Proteins*, ed. P. F. Fox and P. L. H. McSweeney, Kluwer Academic, Plenum, 2002, pp. 233–276.
29 T. Coviello, K. Kajiwara, W. Burchard, M. Dentini and V. Crescenzi, *Macromolecules*, 1986, **19**, 2826–2831.
30 M. Milas, W. F. Reed and S. Printz, *Int. J. Biol. Macromol.*, 1996, **18**, 211–221.
31 G. H. Koenderink, S. Sacanna, D. G. A. L. Aarts and A. P. Philipse, *Phys. Rev. E: Stat., Nonlinear, Soft Matter Phys.*, 2004, **69**, 021804.
32 D. Ausserre, H. Hervet and F. Rondelez, *Phys. Rev. Lett.*, 1985, **54**, 1948–1951.
33 T. J. M. Jeurnink and C. G. de Kruif, *J. Dairy Res.*, 1993, **60**, 139–150.
34 R. K. Dewan, V. A. Bloomfield, A. Chudgar and C. V. Morr, *J. Dairy Sci.*, 1973, **56**, 699–705.
35 P. Zakharov, F. Cardinaux and F. Scheffold, *Phys. Rev. E: Stat., Nonlinear, Soft Matter Phys.*, 2006, **73**, 011413.
36 D. A. Weitz and D. J. Pine, in *Dynamic Light Scattering, the Method and Some Applications*, ed. W. Brown, Clarendon Press, 1993, p. 652.
37 A. O. Karlsson, R. Ipsen, K. Schrader and Y. Ardo, *J. Dairy Sci.*, 2005, **88**, 3784–3797.
38 G. H. Koenderink, D. G. A. L. Aarts, V. W. A. de Villeneuve, A. P. Philipse, R. Tuinier and H. N. W. Lekkerkerker, *Biomacromolecules*, 2003, **4**, 129–136.
39 R. H. Colby, *Rheol. Acta*, 2010, **49**, 425–442.
40 G. Cuvelier and B. Launay, *Carbohydr. Polym.*, 1986, **6**, 321–333.
41 H. C. Lee and D. A. Brant, *Macromolecules*, 2002, **35**, 2223–2234.
42 M. Milas, M. Rinaudo, M. Knipper and J. L. Schuppiser, *Macromolecules*, 1990, **23**, 2506–2511.
43 Y. Takada, T. Sato and A. Teramoto, *Macromolecules*, 1991, **24**, 6215–6219.
44 J. O. Carnali, *J. Appl. Polym. Sci.*, 1991, **43**, 929–941.
45 M. Milas, M. Rinaudo, R. Duplessix, R. Borsali and P. Lindner, *Macromolecules*, 1995, **28**, 3119–3124.
46 B. Hinner, M. Tempel, E. Sackmann, K. Kroy and E. Frey, *Phys. Rev. Lett.*, 1998, **81**, 2614–2617.
47 M. Tassieri, R. M. L. Evans, L. Barbu-Tudoran, G. N. Khaname, J. Trinick and T. A. Waigh, *Phys. Rev. Lett.*, 2008, **101**, 198301.
48 T. G. Mason, *Rheol. Acta*, 2000, **39**, 371–378.
49 D. C. Morse, *Macromolecules*, 1998, **31**, 7044–7067.
50 C. F. Schmidt, M. Barmann, G. Isenberg and E. Sackmann, *Macromolecules*, 1989, **22**, 3638–3649.
51 H. Hinsch, J. Wilhelm and E. Frey, *Eur. Phys. J. E*, 2007, **24**, 35–46.